Physica E 52 (2013) 8–13

Contents lists available at SciVerse ScienceDirect

Physica E

journal homepage: www.elsevier.com/locate/physe

Efficiency droop improvement for InGaN-based light-emitting diodes with gradually increased In-composition across the active region

Jinliang Xu [a,*], Tianhu Wang [b]

[a] Beijing Key Laboratory of New and Renewable Energy, North China Electric Power University, Beijing 102206, China
[b] Beijing Key Laboratory of Multiphase Flow and Heat Transfer, North China Electric Power University, Beijing 102206, China

HIGHLIGHTS

- The internal quantum efficiency and output power performance of light-emitting diodes with gradually increased In-composition $In_xGa_{1-x}N$ barriers were studied.
- The reference structure with GaN barriers, structure A with constant In-composition InGaN barriers and structure B with gradually increased In-composition $In_xGa_{1-x}N$ barriers were chosen for comparison investigation.
- The output power is increased by 28% for the structure B compared with the structure A at 180 mA. The improved performance is caused by the enhanced electron confinement and increased hole injection efficiency.

ARTICLE INFO

Article history:
Received 19 November 2012
Received in revised form
8 March 2013
Accepted 9 March 2013
Available online 29 March 2013

Keywords:
Light-emitting diode
Efficiency droop
Quantum barrier
Indium composition

ABSTRACT

The gradually increased In-composition barriers were proposed to synthesize advantages of low polarization of InGaN barriers and high barrier height of GaN barriers. The reference structure with GaN barriers, the structure A with constant In-composition InGaN barriers and the structure B with gradually increased In-composition $In_xGa_{1-x}N$ barriers were chosen. The light-emitting diodes were numerically studied. It is found that the structure B has the best performance. The output power is increased by 28% for structure B compared with structure A at 180 mA. The improved performance is caused by the enhanced electron confinement and increased hole injection efficiency.

1. Introduction

The III-nitride light-emitting diodes (LEDs) have wide applications in full color display, back lighting and general illumination, etc. [1–4]. However, the InGaN LEDs possess the shortcoming of efficiency droop at high injection current [3,4], forming the obstacle to develop the high power LEDs. Even though several mechanisms for the LED efficiency droop have been recommended, the major mechanism is not fully understood yet. It is commonly recognized that electron leakage and poor hole injection efficiency majorly contribute to the reduced internal quantum efficiency (IQE) [3–11]. Electrons have small effective mass to yield high mobility, thus they can transport in multiple quantum wells (MQWs) easily and even overflow from the electron blocking layer (EBL) to the p-type layer [6,12]. Different from electrons, holes are difficult to transport into MQWs due to their low mobility [7,12] and the potential barrier obstacle of EBL under polarization fields [8]. A set of strategies are recommended to enhance the electron confinement [3–6] and increase the hole injection efficiency [7–10]. The modified designs of EBL [6,8,11], barriers [12–16], last barrier [5,9,10,17] and MQWs [18–21] belong to these strategies.

Usually, the active region of an LED consists of InGaN/GaN MQWs and followed by a p-doped AlGaN EBL. A large lattice mismatch occurs at the InGaN/GaN and the last barrier/EBL interfaces, creating polarization charges and strong band bending to deteriorate the carrier confinement. Under such circumstances, the electron leakage becomes serious. The polarization effect between the well and barrier could be weakened by replacing the GaN barriers with the InGaN barriers [12,14,16]. On the other hand, however, the potential height for carrier confinement is reduced due to the small energy band gap of InGaN. In this work, the gradually increased In-composition $In_xGa_{1-x}N$ barrier was proposed to synthesize the advantages of low polarization effect of InGaN barriers and high barrier height effect of GaN barriers.

* Corresponding author. Tel./fax: +86 10 61772268.
E-mail address: xjl@ncepu.edu.cn (J. Xu).

1386-9477/$ - see front matter © 2013 Elsevier B.V. All rights reserved.
http://dx.doi.org/10.1016/j.physe.2013.03.004

The concept reaches the following targets: (1) the quantum barrier near the n-type layer keeps the GaN's high barrier to confine electrons; (2) the polarization at the interfaces is weakened near the p-type layer. Therefore, the efficiency droop is significantly improved compared with LEDs having the GaN barriers and constant In-composition InGaN barriers.

2. Parameters and models

A reference LED structure with GaN barriers was chosen for comparison. Initially a 100-μm-thick *c*-plane sapphire substrate was prepared. Before the growth of InGaN/GaN MQWs, a 50-nm-thick un-doped GaN buffer layer and a 3-μm-thick Si-doped n-type GaN layer (n-doping$=5\times10^{18}$ cm^{-3}) were deposited on the substrate consecutively. The active region consists of five 2-nm-thick $In_{0.15}Ga_{0.85}N$ quantum wells, separated by six 10-nm-thick GaN barriers. A 20-nm-thick p-type $Al_{0.15}Ga_{0.85}N$ EBL (p-doping $=1\times10^{18}$ cm^{-3}) and a 200-nm-thick p-type GaN cap layer (p-doping$=1.2\times10^{18}$ cm^{-3}) were on the top of the active region. The reference structure had a size of 300 μm × 300 μm. The structures A, B and the reference structure are identical with each other, except the constant In-composition InGaN barriers (In-composition $x=0.05$ in each barrier) for the structure A and the gradually increased In-composition $In_xGa_{1-x}N$ barriers for the structure B. In the active region of structure B, In-composition in the first and last barriers are $x=0.00$ and $x=0.05$ respectively. The In-composition was gradually increased with each step of 0.01 among the two neighboring barriers. Fig. 1 shows the In-composition profiles in the active region of the three LED structures.

The LED optical and electrical properties were numerically investigated with the APSYS simulation program [22] (Crosslight Software Inc.), which solves Poisson's equation, current continuity equations, carrier transport equation, quantum mechanical wave equation and photon rate equation. The non-radiative recombination processes and current leakage are taken into account. The Shockley-Read-Hall (SRH) recombination lifetime is set to be 100 ns. The internal absorption within the LED device and the light extraction efficiency are assumed to 500 m^{-1} and 78%, respectively.

APSYS employs the 6×6 $k\cdot p$ model to caculate the energy band structures, which was developed by Chuang and Chang [23,24]. The band gap energy of InN, GaN, and AlN as a function of temperature T can be expressd by the Varshni formula [25]:

$$E_g(T)=E_g(0)-\frac{\alpha T^2}{T+\beta}, \quad (1)$$

where $E_g(T)$ is the band gap energy at temperature T, $E_g(0)$ is the band gap energy at 0 K, α and β are the material related constants. The values of E_g (0), α, and β for InN, GaN, and AlN are listed in Table 1. The temperature is set to be 300 K in the simulation. For ternary alloys of InGaN and AlGaN, the band gap energies can be expressed as follows [25]:

$$E_g(In_xGa_{1-x}N)=E_g(InN)x+E_g(GaN)(1-x)-b(In_xGa_{1-x}N)x(1-x), \quad (2)$$

$$E_g(Al_xGa_{1-x}N)=E_g(AlN)x+E_g(GaN)(1-x)-b(Al_xGa_{1-x}N)x(1-x), \quad (3)$$

where E_g ($In_xGa_{1-x}N$) and E_g ($Al_xGa_{1-x}N$) are the band gap energies of $In_xGa_{1-x}N$ and $Al_xGa_{1-x}N$, the bowing parameters for $In_xGa_{1-x}N$ and $Al_xGa_{1-x}N$ are 1.43 and 1.0, respectively. Other material parameters of the LEDs used in the simulation are cited from Ref. [26].

The charge density induced by the spontaneous and piezoelectric polarization at the hetero interface can be calculated by the method developed by Fiorentini et al. [27]. The spontaneous polarization of the ternary nitride alloys can be expressed as:

$$P_{sp}(In_xGa_{1-x}N)=-0.0413x-0.0339(1-x)+0.0378x(1-x), \quad (4)$$

$$P_{sp}(Al_xGa_{1-x}N)=-0.0898x-0.0339(1-x)+0.0191x(1-x). \quad (5)$$

The piezoelectric polarization of ternary alloys can be expressed as:

$$P_{pz}(In_xGa_{1-x}N)=P_{pz}(InN)x+P_{pz}(GaN)(1-x), \quad (6)$$

$$P_{pz}(Al_xGa_{1-x}N)=P_{pz}(AlN)x+P_{pz}(GaN)(1-x), \quad (7)$$

where

$$P_{pz}(InN)=-1.373\varepsilon+7.559\varepsilon^2, \quad (8)$$

$$P_{pz}(GaN)=-0.918\varepsilon+9.541\varepsilon^2, \quad (9)$$

$$P_{pz}(AlN)=-1.808\varepsilon+5.642\varepsilon^2(\varepsilon<0) \quad (10)$$

$$P_{pz}(AlN)=-1.808\varepsilon-7.888\varepsilon^2(\varepsilon>0). \quad (11)$$

The basal strain for the alloy matched to the GaN layer is defined as:

$$\varepsilon=\frac{(a_{sub}-a)}{a}, \quad (12)$$

where a_{sub} and a are the lattice constants of the GaN and alloy layers, respectively. The total polarization is the sum of the spontaneous and piezoelectric polarization.

The Caughey–Thomas approximation [28] is employed in the simulation for the carrier mobility as a function of carrier density

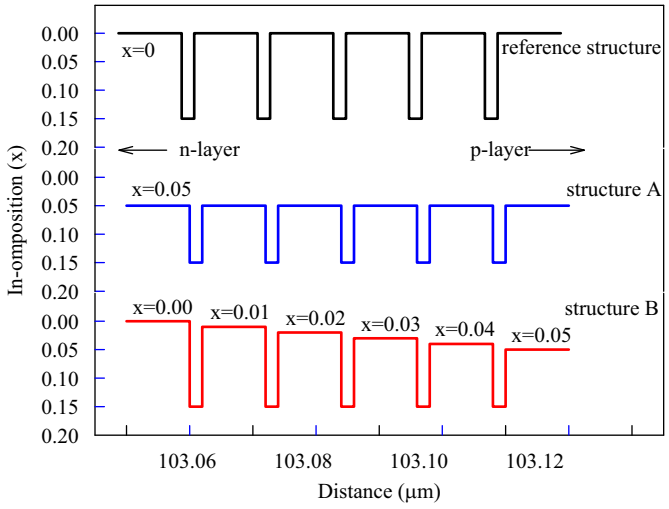

Fig. 1. The In-composition distributions in the active region among the three LED structures.

Table 1
Material parameters used in the simulation for the binary semiconductor compound energy band gaps.

Parameters	InN	GaN	AlN
E_g (0) (eV)	0.735	3.507	6.23
α (meV/K)	0.245	0.909	1.799
β (K)	624	830	1462

Table 2
Material parameters used in the simulation for carrier mobility.

Parameters	AlGaN	InGaN
$\mu_{max,n}$ ($cm^2\,V^{-1}\,s^{-1}$)	306	684
$\mu_{min,n}$ ($cm^2\,V^{-1}\,s^{-1}$)	132	386
$N_{ref,n}$ (cm^{-3})	1×10^{17}	1×10^{17}
α_n	0.29	1.37
$\mu_{max,p}$ ($cm^2\,V^{-1}\,s^{-1}$)	10	2
$\mu_{min,p}$ ($cm^2\,V^{-1}\,s^{-1}$)	10	2
$N_{ref,p}$ (cm^{-3})	3×10^{17}	2.75×10^{17}
α_p	0.395	0.395

which can be expressed as follows:

$$\mu_i(N) = \mu_{min,i} + \frac{\mu_{max,i} - \mu_{min,i}}{1.0 + (N/N_{ref,i})^{\alpha,i}}, \tag{13}$$

where i denotes either electron or hole, all parameters in the formula are listed in Table 2.

3. Results and discussion

In order to verify the correct numerical simulation for the reference structure and proposed new structure, we performed the comparison between our present simulation results with those reported in Ref. [12]. Kuo et al. [12] investigated the advantages of blue LEDs with InGaN barriers. They reported the *L–I* curves, carrier concentrations in quantum wells, energy band diagrams, and internal quantum efficiency. They pointed out that the InGaN/InGaN LED has better performance over its conventional InGaN/GaN counterpart due to the enhancement of electron confinement, the reduced polarization effect between the barrier and well, and the lower potential barrier height for the holes to transport in the active region. They also showed that the efficiency droop is markedly improved when the traditional GaN barriers are replaced by InGaN barriers.

We used the software and parameter setting exactly identical to those in Ref. [12]. The experimental and simulated light–current–voltage (*L–I–V*) performance curves of the original InGaN/GaN structure were plotted in Fig. 2. It is found that our present simulation results matched the experimental data and simulation results by Kuo et al. [12] well. This provides the evidence that our present numerical simulations are correct and acceptable for the investigation of new LED structure studied in this paper. The LED performance may be sensitive to parameter settings. The material parameters for this new LED structure are similar to those specified by Refs. [9,12,26].

Fig. 3 shows the energy band diagrams and quasi-Fermi levels of the LEDs for the three structures with an injection current of 180 mA. For the reference structure with GaN barriers, the band bending in the active region and at the last barrier/EBL interface was significant, caused by the strong piezoelectric field induced by the polarization charges at these interfaces [see Fig. 3(a)]. This effect is not helpful to suppress the electron leakage due to the reduced effective potential barrier height of the AlGaN EBL. The effective barrier height is defined as the potential difference between the maximum energy of the EBL and the quasi-Fermi level in front of the EBL. Structure A with constant In-composition InGaN barriers increases the effective barrier height of the EBL for the electron confinement and weakens the potential height in the valance band [see Fig. 3(b)], which is helpful for the holes transportation into the active region [8]. The structure B with gradually increased In-composition $In_xGa_{1-x}N$ barriers effectively confines electrons in the active region. The effective potential height of 223 meV for the structure B [see Fig. 3(c)] is the highest among the three structures. Such value is 189 meV for the reference structure and 204 meV for structure A. Besides, structure B with gradually increased In-composition $In_xGa_{1-x}N$ barriers flattens the last two barriers in the valence band and decreases the effective potential height for holes. Structure B yields the smallest effective potential height for holes of 224 meV, compared with 261 meV for the reference structure and 226 meV for the structure A. This is due to the slightly weakened polarization near

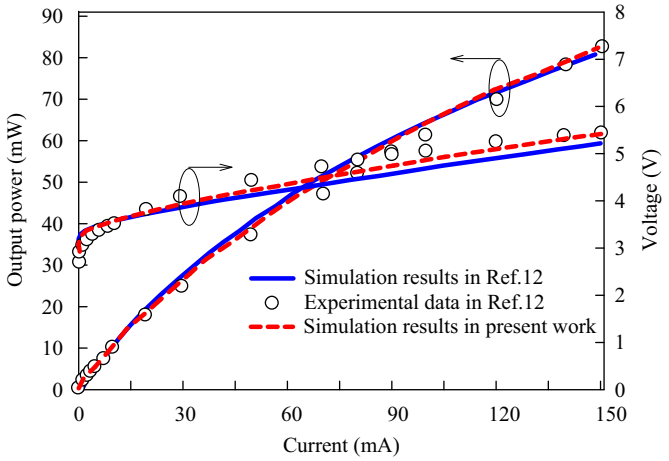

Fig. 2. The comparison between our present numerical simulation with the experimental data and simulation results given by Ref. [12].

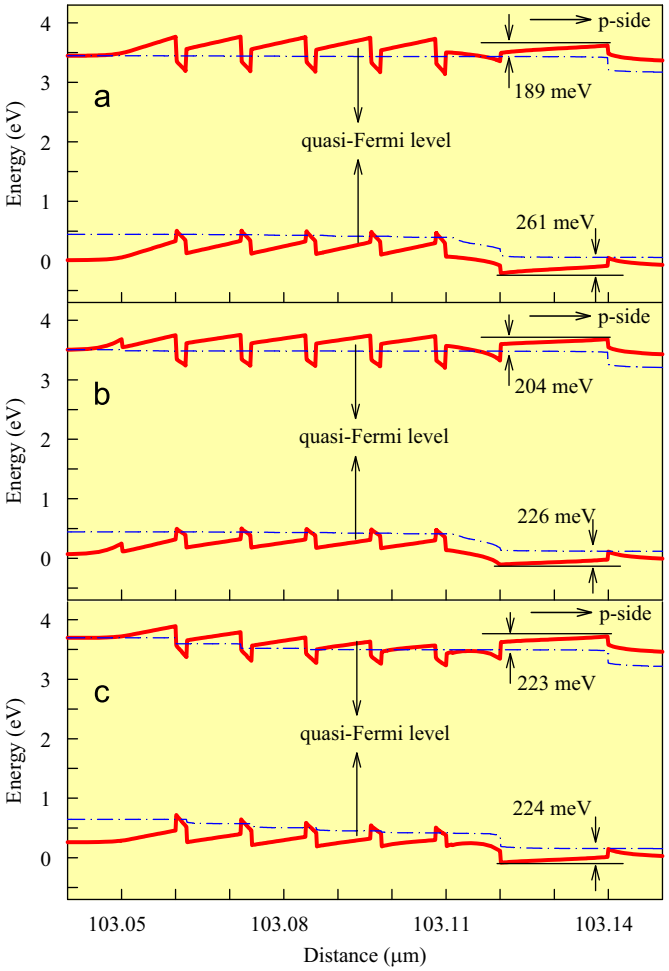

Fig. 3. The energy band diagrams for the three LED structures at 180 mA. (a) reference structure, (b) structure A and (c) structure B.

the last barrier/EBL interface, leading to the improved hole injection efficiency for structure B [4]. The difference between the quasi-Fermi level and the valence band becomes minimal in the last two QWs for structure B among the three structures indicating the improved hole injection efficiency. Combining the two factors of the enhanced electron confinement of the EBL and the improved holes injection efficiency, the quantum efficiency can be increased when gradually increased In-composition $In_xGa_{1-x}N$ barriers are used.

Fig. 4 shows electron current densities over the active region for the three structures at the injection current of 180 mA. Electrons are injected from n-layers into MQWs and recombined with holes there, yielding the decreased electron current densities along the transportation distance. It is noted that the electron leakage current overflowing from the active region to the p-layers is significant for the reference structure. Structure A with the constant In-composition InGaN barrier decreases the electron leakage current. Structure B with gradually increased In-composition barriers further suppresses the electron leakage current efficiently. Before holes are injected into the active region, the non-radiative recombination of holes with the leaked electrons outside of the active region is minimized, thus the hole injection efficiency is increased for structure B.

Fig. 5 shows carrier concentrations for the three structures at the injection current of 180 mA. For the reference structure shown in Fig. 5(a), carrier concentrations in QWs are lower and most carriers are populated in the last QW due to the serious electron current leakage and low holes mobility. Structure A possesses higher carrier concentrations in QWs [see Fig. 5(b)], due to the decreased polarization effect in QWs and improved effective potential height at the last barrier/EBL interface [12]. Fig. 5(c) shows the significantly increased carrier concentrations in the last

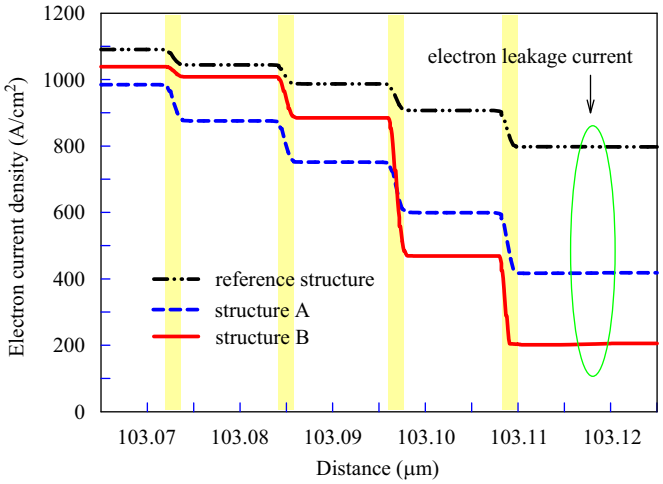

Fig. 4. The electron current densities over the active region for the three LED structures at 180 mA.

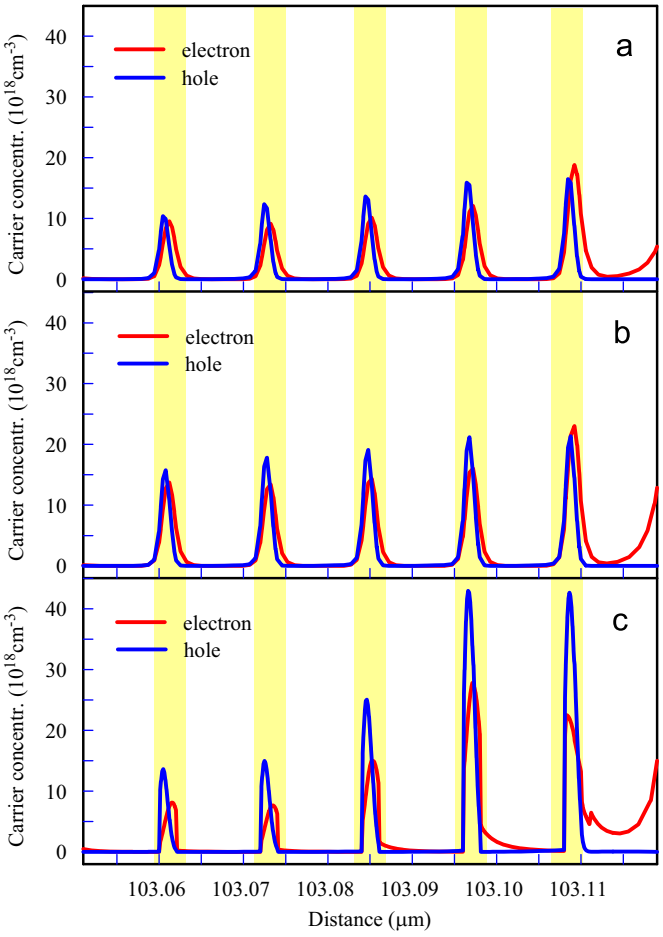

Fig. 5. The carrier concentrations over the active region for the three structures at 180 mA. (a) reference structure, (b) structure A and (c) structure B.

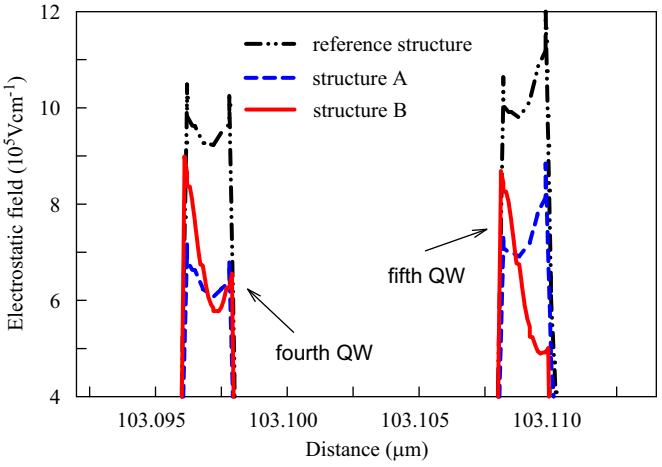

Fig. 6. The electrostatic fields in the last two quantum wells for the three structures at 180 mA.

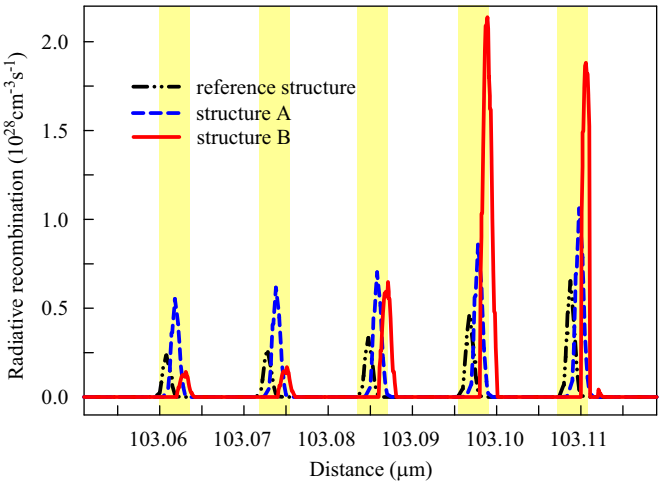

Fig. 7. The radiative recombination rates in the active region of the three LEDs at 180 mA.

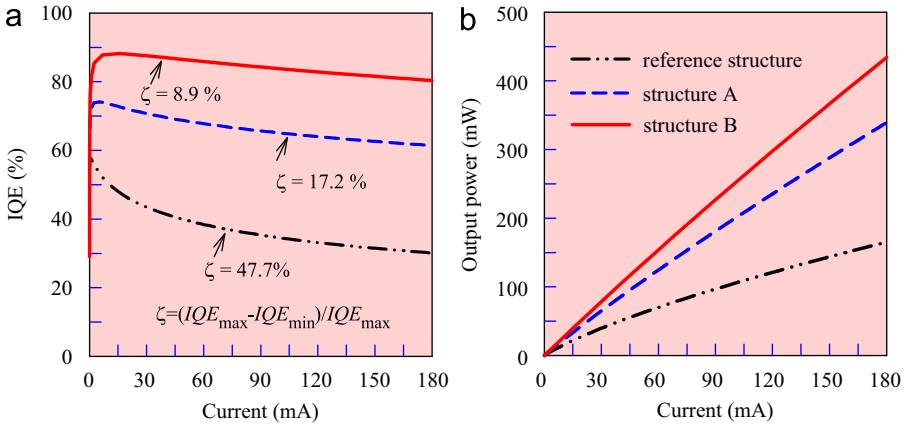

Fig. 8. The (a) internal quantum efficiency and (b) output power as a function of injection current of the three LEDs.

three QWs next to the p-type layer for the structure B. Compared with the structure A, the average electron concentrations are increased from 16.1×10^{18} cm^{-3} to 16.2×10^{18} cm^{-3}, and the average hole concentrations are increased from 19.0×10^{18} cm^{-3} to 27.9×10^{18} cm^{-3} in the active region for the structure B. Moreover, the hole concentrations are quite uniform in the last two QWs, which means improved hole transport capability near the p-type layer [14]. Therefore, the electron leakage can be decreased due to the enhanced electron confinement and increased hole injection efficiency in QWs.

Fig. 6 plots the electrostatic fields in the last two quantum wells at an injection current of 180 mA. The quantum confined Stark effect in the quantum wells induced by the internal electric field can restrict the radiative recombination rate through the deterioration of wave function spatial overlap between electrons and holes. Thus, the internal quantum efficiency is deteriorated [19,29,30]. As indicated in Fig. 6, the electrostatic fields in the last two quantum wells are reduced when the In-composition gradually increased barriers are used, indicating the better wave function overlap between electrons and holes. One reason of the alleviated electrostatic fields are responsible for the better lattice match near the EBL region, which results in smaller polarization charges at the InGaN/InGaN interfaces [16]. On the other hand, the large electrostatic fields in the last two quantum wells could also be compensated by the strong screening effect due to the large carrier concentrations in the last two quantum wells [see Fig. 5]. Therefore, the enhanced electron and hole wave functions overlap together with the increased carrier concentration in the active region improve the radiative recombination markedly.

Fig. 7 shows radiative recombination rates for the three structures, noting that the horizontal coordinates are slightly shifted for structures A and B for easy comparison purpose. The radiative recombination rate for structure B is 2.54 times of that for the reference structure, and 1.31 times of that for structure A, further improving the optical performance. Again, we see that the radiative rates are significantly increased in the last two QWs for structure B, consistent with the carrier concentrations among different QWs [see Fig. 5(c)].

Fig. 8 shows the simulated IQEs and output powers versus injection currents for the three structures. Over the injection current range, structure B has the largest IQE and light out put power. We define the efficiency droop ratio of IQE as $\zeta = (IQE_{max} - IQE_{min})/IQE_{max}$, where IQE_{max} and IQE_{min} are the maximum and minimum internal quantum efficiencies, respectively. The efficiency droop ratio reaches 47.7% for the reference structure. It is decreased to 17.2% for structure A with constant In-composition InGaN barriers, and attains the smallest value of 8.9% for structure B with gradually increased In-composition $In_xGa_{1-x}N$ barriers. The increased IQEs directly lead to the raised output power. At the injection current of 180 mA, the output power for structure B is 2.63 times of that for the reference structure, and 1.28 times of that for structure A. In other words, the output power is increased by 28% if gradually increased In-composition barriers replace the constant In-composition barriers.

4. Conclusions

In summary, LEDs with GaN barriers, constant In-composition InGaN barriers, and gradually increased In-composition $In_xGa_{1-x}N$ barriers are numerically studied. The gradually increased In-composition $In_xGa_{1-x}N$ barriers greatly change the energy band near the last two QWs and increase the effective potential height of the EBL, enhancing the electron confinement and increasing the holes injection efficiency from the p-type layer into the active region. This effect enlarges the radiative recombination rate in quantum wells to significantly increase IQEs and light output powers. The results also indicate that the polarization electrostatic field in the last two quantum wells of the LED with In-composition gradually increased barriers is alleviated when compared to the reference LED, improving the wave function overlaps between electrons and holes. The gradually increased In-composition $In_xGa_{1-x}N$ structure is recommended to be used at high injection currents.

Acknowledgments

This work was financially supported by the National Natural Science Foundation of China (U1034004, 50825603 and 51210011).

References

[1] M.R. Krames, O.B. Shchekin, R. Mueller-Mach, G.O. Mueller, L. Zhou, G. Harbers, M.G. Craford, Journal of Display Technology 3 (2007) 160.
[2] L.E. Cai, B.P. Zhang, J.Y. Zhang, C.M. Wu, F. Jiang, X.L. Hu, M. Chen, Q.M. Wang, Physica E 43 (2010) 289.
[3] M.H. Kim, M.F. Schubert, Q. Dai, J.K. Kim, E.F. Schubert, J. Piprek, Y. Park, Applied Physics Letters 91 (2007) 183507.
[4] M.F. Schubert, J. Xu, J.K. Kim, E.F. Schubert, M.H. Kim, S. Yoon, S.M. Lee, C. Sone, T. Sakong, Y. Park, Applied Physics Letters 93 (2008) 041102.
[5] J.R. Chen, T.C. Lu, H.C. Kuo, K.L. Fang, K.F. Huang, C.W. Kuo, C.J. Chang, C.T. Kuo, S.C. Wang, IEEE Photonics Technology Letters 22 (2010) 860.
[6] S. Choi, H.J. Kim, S.S. Kim, J. Liu, J. Kim, J.H. Ryou, R.D. Dupuis, A.M. Fischer, F.A. Ponce, Applied Physics Letters 96 (2010) 221105.
[7] X. Ni, Q. Fan, R. Shimada, Applied Physics Letters 93 (2008) 171113.
[8] C.H. Wang, C.C. Ke, C.Y. Lee, S.P. Chang, W.T. Chang, J.C. Li, Z.Y. Li, H.C. Yang, H.C. Kuo, T.C. Lu, S.C. Wang, Applied Physics Letters 97 (2010) 261103.
[9] Y.K. Kuo, M.C. Tsai, S.H. Yen, T.C. Hsu, Y.J. Shen, IEEE Journal of Quantum Electronics 46 (2010) 1214.

[10] C.S. Xia, Z.M. Simon, W. Lu, Z.H. Zhang, Y. Sheng, L.W. Cheng, Applied Physics Letters 99 (2011) 233501.
[11] H. Hirayama, Y. Tsukada, T. Maeda, N. Kamata, Applied Physics Express 3 (2010) 031002.
[12] Y.K. Kuo, J.Y. Chang, M.C. Tsai, S.H. Yen, Applied Physics Letters 95 (2009) 011116.
[13] C.H. Wang, S.P. Chang, P.H. Ku, J.C. Li, Y.P. Lan, C.C. Lin, H.C. Yang, H.C. Kuo, T.C. Lu, S.C. Wang, C.Y. Chang, Applied Physics Letters 99 (2011) 171106.
[14] Y.K. Kuo, T.H. Wang, J.Y. Chang, M.C. Tsai, Applied Physics Letters 99 (2011) 091107.
[15] P.M. Tu, C.Y. Chang, S.C. Huang, C.H. Chiu, J.R. Chang, W.T. Chang, D.S. Wuu, H.W. Zan, C.C. Lin, H.C. Kuo, C.P. Hsu, Applied Physics Letters 98 (2011) 211107.
[16] Y.K. Kuo, M.C. Tsai, S.H. Yen, T.C. Hsu, Y.J. Shen, IEEE Journal of Selected Topics in Quantum Electronics 15 (2009) 1115.
[17] S.H. Yen, M.L. Tsai, M.C. Tsai, S.J. Chang, Y.K. Kuo, IEEE Photonics Technology Letters 22 (2010) 1787.
[18] H. Zhao, G. Liu, X.H. Li, G.S. Huang, J.D. Poplawsky, S.T. Penn, V. Dierolf, N. Tansu, Applied Physics Letters 95 (2009) 061104.
[19] H. Zhao, R.A. Arif, N. Tansu, IEEE Journal of Selected Topics in Quantum Electronics 15 (2009) 1104.
[20] Y.J. Lee, C.H. Chen, C.J. Lee, IEEE Photonics Technology Letters 22 (2010) 1506.
[21] C.T. Liao, M.C. Tsai, B.T. Liou, S.H. Yen, Y.K. Kuo, Journal of Applied Physics 108 (2010) 063107.
[22] APSYS by Crosslight Software Inc., Burnaby, Canada. ⟨http://www.crosslight.com⟩.
[23] S.L. Chuang, C.S. Chang, Physical Review B 54 (1996) 2491.
[24] S.L. Chuang, C.S. Chang, Semiconductor Science and Technology 12 (1997) 252.
[25] I. Vurgaftman, J.R. Meyer, L.R. Ram-Mohan, Journal of Applied Physics 89 (2001) 5815.
[26] I. Vurgaftman, J.R. Meyer, Journal of Applied Physics 94 (2003) 3675.
[27] V. Fiorentini, F. Bernardini, O. Ambacher, Applied Physics Letters 80 (2002) 1204.
[28] C.M. Caughey, R.E. Thomas, Proceedings of the IEEE 55 (1967) 2192.
[29] H.P. Zhao, G.Y. Liu, J. Zhang, J.D. Poplawsky, V. Dierolf, N. Tansu, Optics Express 19 (2011) A991.
[30] Y. Li, B. Liu, R. Zhang, Z. Xie, Y. Zheng, Physica E 44 (2012) 821.